Energy Technology
Generation, Conversion, Storage, Distribution
www.entechnol.de

All-Sprayable Hierarchically Nanostructured Conducting Polymer Hydrogel for Massively Manufactured Flexible All-Solid-State Supercapacitor

Yu Han, Xiang Chu, Haitao Zhang,* Haichao Huang, Guo Tian, Zixing Wang, Bingni Gu, Ningjun Chen, Wen Deng, Weili Deng, and Weiqing Yang*

The low-cost processing and uniquely structured design of conducting polymer hydrogels (CPHs), with the advantages of both conducting polymers and 3D frameworks, are the keys to their wide commercial application in next-generation flexible solid supercapacitors. Herein, an all-sprayable hierarchically nanostructured polyaniline–phytic acid conducting polymer hydrogel (pp-CPHs) for upgradable art patterns and massively manufactured supercapacitor electrodes is presented. Ascribing to fully anticipating the efficient electrode–electrolyte interface of 3D porous nanostructures constructed by interconnected nanorods, the pp-CPH-based flexible all-solid-state supercapacitors exhibit an excellent areal capacitance of 91 mF cm^{-2} at a current density of 1 mA cm^{-2} and a drastically improved cycling stability with 93.5% capacitance retention after 10 000 cycles at 5 mA cm^{-2}. In addition, the electrochemical performance of this device can be constantly maintained under various mechanical loadings such as bending and twisting. Also, this device shows a remarkable integration ability from its universal tandem and parallel connections. Unambiguously, these aforementioned merits of pp-CPH-based flexible all-solid-state supercapacitors make it an ideal maneuver for the massive fabrication of flexible power supply.

1. Introduction

Research interests on the low-cost manufacturing process, lightweight design, and considerable mechanical flexibility of power sources are rising continuously due to the proliferation of portable and flexible electronics.[1] Among various power sources, flexible supercapacitor is one of the most promising candidates attributed to its fast charge–discharge rate, modest energy density, high power density, excellent cycling stability, along with the potential to achieve a relatively high energy density close to traditional batteries.[2] As an emerging class of flexible supercapacitors, flexible all-solid-state supercapacitor holds a great promise for power supplies ascribing to its excellent safety and remarkable flexibility. Notably, a number of striking improvements in the performance of flexible all-solid-state supercapacitors have been achieved through recent advancements in electrode materials.[3] Currently, such electrodes are ordinarily made of electrochemically active carbonaceous materials, transition metal oxides, conductive polymers (CPs), and the composites of these materials.[4] Among them, CPs have attracted a great attention due to their soft nature and intrinsically high pseudocapacitance.[5] Relevant to CPs, previous research mostly tend to either design unique nanostructures or show synergistic effect between CPs and other materials (e.g., carbonaceous materials and transition metal oxides),[6] but studies on derivatives of CPs have rarely been reported to date. For derivatives of CPs such as conducting polymer hydrogels (CPHs), Li et al.[7] have recently reported a novel method for synthesizing the polyaniline–polyvinyl alcohol hydrogel by the supramolecular assembly of polyaniline and polyvinyl alcohol through a dynamic boronated bond. Interestingly, the flexibility supercapacitors based on the polyaniline–polyvinyl alcohol hydrogel drastically provide a large capacitance (306 mF cm^{-2} and 153 F g^{-1}). Therefore, this CPH show a promising potential in the fabrication of high-performance flexible solid-state supercapacitors.

3D CPH, a type of monolithic scaffold superstructures comprising CPs nanoparticles or nanosheets, not only inherit wonderful properties of CPs such as relatively high conductivity,[8] considerable softness,[9] unique conjugated chain structure,[10] and intrinsic large pseudocapacitance[11] but also offer 3D interconnected networks with unique properties of large surface area, outstanding mechanical durability, and high ion-transmission efficiency.[12] Due to the fact that the solid phase of CPHs is completely surrounded by large amounts of the liquid phase, the electrochemical materials can be fully utilized.[3a,13]

Y. Han, X. Chu, H. Zhang, H. Huang, G. Tian, Z. Wang, B. Gu, N. Chen, W. Deng, W. Deng, W. Yang
Key Laboratory of Advanced Technologies of Materials (Ministry of Education), School of Materials Science and Engineering
Southwest Jiaotong University
Chengdu 610031, P. R. China
E-mail: haitaozhang@swjtu.edu.cn; wqyang@swjtu.edu.cn
W. Yang
State Key Laboratory of Traction Power
Southwest Jiaotong University
Chengdu 610031, China
The ORCID identification number(s) for the author(s) of this article can be found under https://doi.org/10.1002/ente.201801109.

DOI: 10.1002/ente.201801109

Furthermore, the extra surface area and molecular contact of electrode materials and electrolyte can also be achieved benefiting from the swelling behavior of the polymer with water and ions, which leads to the efficient electrochemical process of supercapacitors (SCs).[14] These aforementioned advantages incontrovertibly make 3D CPH an ideal electrode candidate for flexible all-solid-state supercapacitors.

In this work, we propose a hierarchically nanostructured polyaniline–phytic acid conducting polymer hydrogels (pp-CPHs) for the massively all-sprayable fabrication of flexible all-solid-state supercapacitors, in which phytic acid is used as both dopant and crosslinker to interact with polyaniline molecular chains to form interconnected networks. Such resultant pp-CPHs exhibit a high conductivity of 0.25 S cm^{-1} and a desirable processability via the spraying technology. Its scanning electron microscopy (SEM) image observably proves a porous foam morphology of the pp-CPH, which is constructed by numerous interconnected nanorods. Consequently, such interconnected nanorods naturally form a continuous electronic transfer phase, and the pores distributed in the networks form unblocked channels for ion and mass transfer.[15] Due to these unique porous nanostructures, the pp-CPH-based flexible all-solid-state supercapacitors exhibit a high areal capacitance of 91 mF cm^{-2} at 1 mA cm^{-2}. Also, this device demonstrates an excellent capacitive performance with only 6.5% decay after 10 000 cycles at a scan rate of 5 mA cm^{-2}, which is much higher than most of the previously reported CPs-based materials.[3a,16] In addition, the electrochemical performance of this device can be maintained under various mechanical loadings such as bending and twisting. Evidently, these aforementioned features make the as-prepared device a promising power supply candidate for future wearable electronics and flexible electronics.

2. Experimental Section

2.1. Synthesis of pp-CPHs

The preparation of pp-CPHs is as follows: 2 mL deionized (DI) water was slowly added into a mixture solution of 0.458 mL (5 mmol) aniline in 0.921 mL (1 mmol) of phytic acid (50%, wt/wt in water); then, a mixture solution of 0.286 g (1.25 mmol) ammonium persulfate in 1 mL DI water was added, followed by stirring for quick mixing at 0 °C water bath about 0.5 h. To remove excess acid and by-products from polymerization, as-prepared pp-CPHs were purified by immersing in DI water with a semipermeable membrane for 24 h. Successively, as-prepared pp-CPHs were taken out from the semipermeable membrane for the following experiments.

2.2. Synthesis of Gel Electrolyte

H_2SO_4 (10 g) was slowly added into 100 mL DI water followed by mixing 10 g PVA (1799 type). The whole mixture was stirred for 1 h at 85 °C water bath, and then a clear PVA/H_2SO_4 gel electrolyte was obtained.

2.3. Fabrication of Flexible All-Solid-State Supercapacitors

The PET film was carved into a 1 × 1 cm square via the ultraviolet laser marking technology (UV-3S, China), and then a layer of gold was deposited on the PET film via magnetron sputtering (TRP450, China). Our device was fabricated by spray-coating of the pp-CPHs as the active material on an area of 1 × 1 cm^2. To dry each coated layer immediately, a commercial hair-dryer was turned on after spraying a layer of hydrogel. We can increase or decrease the number of spray cycles to control the film thickness. To assemble our device, the as-prepared PVA/H_2SO_4 gel electrolyte was carefully and slowly poured on the two completely dried patterns. The two electrodes were pressed together and left for a few minutes until the gel electrolyte was semi-solidified. Lastly, such pressed electrodes were placed into the mold and packaged with polydimethylsiloxane (PDMS) module glue, and then the mold was fixed with clips and placed in the air for 24 h at room temperature. When the PDMS module glue was curing, the device was successfully prepared by removing the mold.

2.4. Data Processing

The electrochemical tests, including electrochemical impedance spectroscopy (EIS), cyclic voltammetry (CV), and galvanostatic charge–discharge (GCD), were carried out by an electrochemical workstation (CHI660E). The cycle life tests were conducted by an Arbin MSTAT4 multichannel galvanostatic-potentiated instrument (Arbin, USA). The areal capacitance of the devices is calculated from the GCD curves based on Equation (1).

$$C_A = I_s \Big/ \left[S \cdot \left(\frac{dU}{dt} \right) \right] \quad (1)$$

In this case, I_s represents the GCD charge–discharge current density based on the areal parameter (mA), S is the efficient area of the device (cm^2), $\frac{dU}{dt}$ represents the slope of GCD curves.

2.5. Characterizations

The surface morphology of the vacuum-dried powders was observed using a SEM (FEI QUANTA FEG 250, USA) and elemental analysis was conducted via EDX spectroscopy. The SEM sample was prepared by dropping several drops of as-prepared pp-CPHs onto a wafer and drying by a heating station. Transmission electron microscopy (TEM) characterizations were observed using a JEOL JEM-2100F instrument with an accelerating voltage of 200 kV. Subsequently, the X-ray diffraction (XRD) of the samples was carried out with a PANalytical X'Pert Powder diffractometer using Cu Kα radiation between 5° and 80°. Fourier-transformed IR (FTIR) spectra were recorded on a Nicolet 6700 spectrometer (Thermo Fisher Scientific, USA). Raman spectra were obtained from a RM2000 microscopic confocal Raman spectrometer using 632.8 nm laser excitation.

3. Results and Discussion

Each phytic acid molecule can react with PANI by protonating the nitrogen groups on PANI. This cross-linking effect leads

to a rapid gelation and the formation of a mesh-like hydrogel network (**Figure 1**a). Then, we used a spray method to deposit pp-CPHs on the as-prepared gold electrode as an electroactive layer (Figure 1b). To assemble the device, the PVA/H_2SO_4 gel electrolyte was carefully dropped onto the two-separate pp-CPHs electrodes, followed by air-drying for 12 h to evaporate excess water. The final outcome resulted in the pp-CPH-based flexible all-solid-state supercapacitors (Figure 1c). The schematic illustration of the general structure of flexible all-solid-state supercapacitor is shown in Figure 1d. We can see the space available among the macromolecular chains that are formed in the coralline porous architecture. This unique structure provides ion channels for the penetration of the electrolyte, which is very important for establishing a rapid redox reaction and inhibiting the volume effect.[17]

Interestingly, the pp-CPHs have an excellent sprayability. This indicates that using different molds, such an electrode material can be patterned into desired shapes (e.g., high-speed train, giant panda, and school badge) (**Figure 2**a). SEM images of the dehydrated pp-CPHs (Figure 2b) show a porous network structure, which is composed of interconnected coral-like dendritic nanofibers with diameters of 60–100 nm (Figure 2c). The EDS mapping was adopted to further analyze the elemental composition of pp-CPHs (Figure 2d). The results showed that O (≈50.11%), C (≈19.73%), and N (≈17.19%) are the main elements, whereas P (≈12.97%) occupy a smaller proportion. Moreover, a uniform distribution of O, P, C, and N elements could be obviously observed at the same time, which is consistent with the morphology of the pp-CPHs. To further probe the single nanofiber and continuous network structure of pp-CPHs, the TEM characterization method was applied. Figure 2e basically shows the holes between branched nanofibers, which can provide ion channels for electrolyte penetration. Therefore, pp-CHPs show a better performance as electrode materials for supercapacitors. Figure 2f,g shows TEM images of single pp-CHPs nanofibers at different amplification rates, with a diameter of ≈100 nm. It can also be observed that polyaniline nanoparticles are uniformly distributed on pp-CHPs nanofibers, which is in good agreement with the results of SEM characterization. Due to the expansion of polyaniline, pp-CHPs nanofibers can provide additional effective surface area between solid and liquid phases during charging and discharging. Attributing to large open channels of micron-scale and nanometer-scale pores within the 3D hierarchical interconnected coral-like dendritic nanofibers, pp-CPHs could further facilitate the transport of electron and electrolyte ions. Consequently, the hierarchical structure could anticipate being more effective than wires and particles for energy storage devices.[18]

The FTIR spectroscopy of pp-CPHs (**Figure 3**a) shows that the salient signatures of pp-CPHs were identical to the emeraldine salt form of PANI. Due to the free-electron conduction in pp-CPHs, the spectral region around 3000–2000 cm^{-1} had a large descending baseline. The bands at 1581 and 1483 cm^{-1} in the FTIR spectrum of dry pp-CPHs were assigned to the benzene ring vibration of PANI, which demonstrates that the chemical structure of pp-CPHs was emeraldine rather than solely the leucoemeraldine or pernigraniline form. The peaks at 1308 and 1152 cm^{-1} were attributed to the C—N stretching vibration with aromatic conjugation and the N=Q=N (Q denotes a quinoid ring) stretching mode, respectively,[19] indicating the presence of PANI in the doped polymer. The bending vibrations of the C—H bonds within the 1,4-disubstituted aromatic ring appear at 818 and 535 cm^{-1}, respectively.[20] FTIR spectra of pp-CPH composites exhibited characteristic bands of PANI, indicating the presence of PANI in the doped polymer.

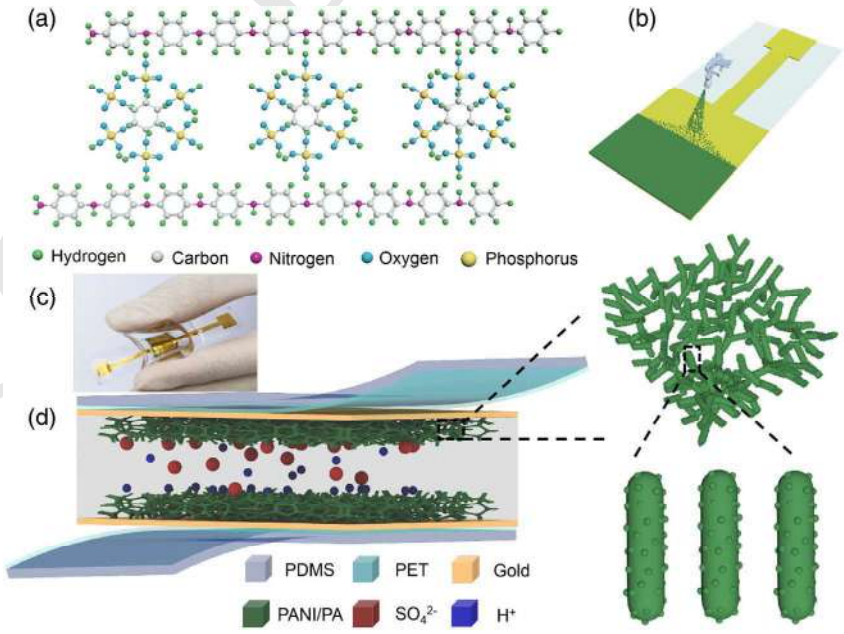

Q6 **Figure 1.** a) A reticulated supramolecular hydrogel formed by cross-linking a PANI molecular chain with a PA molecule. b) Spray-coating of an electroactive pp-CPHs on the gold current collector. c) A fabricated flexible all-solid supercapacitor under its bending state. d) A schematic image of the device structure based on sprayable pp-CPHs.

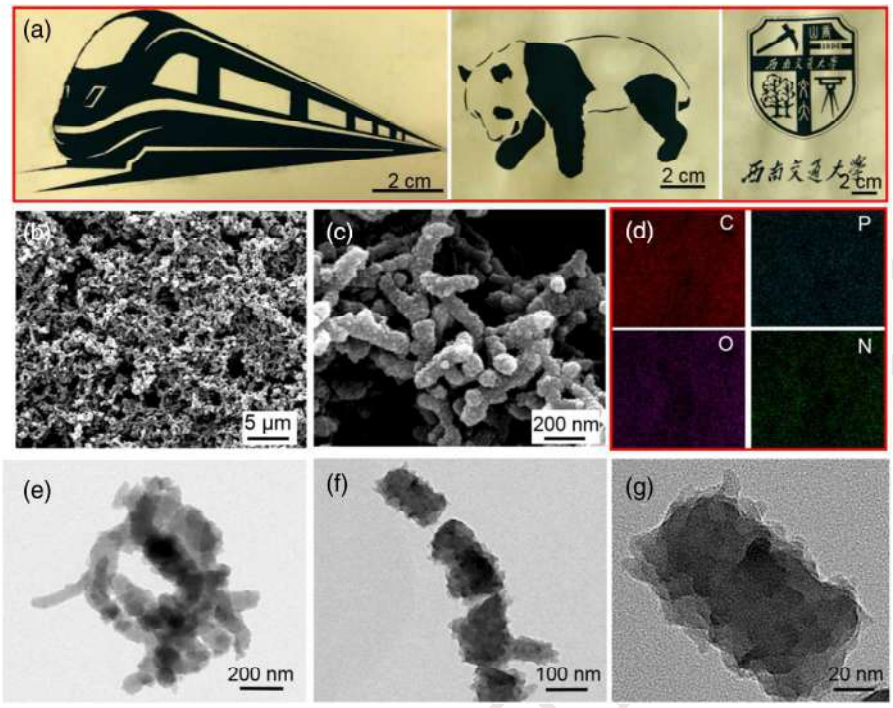

Figure 2. a) Spray display, including the train, giant panda, and southwest jiaotong school emblem. b,c) Representative SEM images of pp-CPHs. d) EDS mapping of pp-CPHs, a general uniform distribution of carbon, nitrogen, and phosphorus can be observed. e–g) TEM images of pp-CPHs.

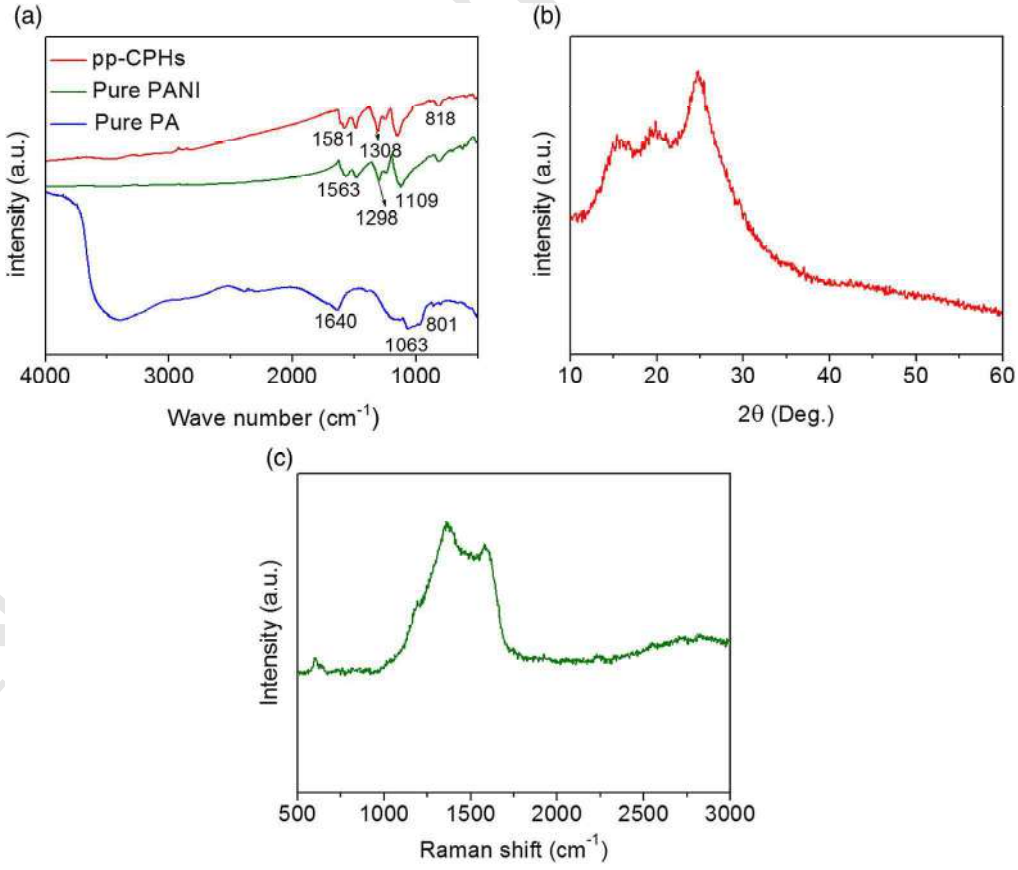

Figure 3. a) FTIR spectra compared among pp-CPHs and PA. b) XRD and c) Raman pattern of pp-CPHs.

The XRD pattern of pp-CPH composites (Figure 3b) displayed the characteristic diffraction peaks centered at 14.9°, 19.8°, and 24.6°. Meanwhile, typical peaks of pure PANI appeared at 2θ degree of about 19.7° and 24.6°, corresponding to (0 2 0) and (2 0 0) crystallographic planes.[21] We thought the peaks of pp-CPHs at 19.8° and 24.6° are corresponding to the PANI component, suggesting that phytic acid-doped PANI did not damage the crystalline structure of the pristine PANI. From the Raman images (shown in Figure 3c), one could observe that the pp-CPH-composited spectrum possesses prominent peaks at around 1370 and 1580 cm^{-1}. The peak of 1370 cm^{-1} belonged to the antisymmetric stretching vibration between C—N and C—C bonds. The peak of 15 800 cm^{-1} originated from the stretching vibration of C=C double bond in the benzene ring.[22]

The electrochemical capacitive behavior of the as-fabricated device is further investigated by EIS. The EIS plots are shown in **Figure 4**a, and the impedance curves are almost parallel to $-Z''$ axis at a low-frequency region, indicating an ideal capacitive behavior of this SC. Figure 4b shows the CV curves of our device at scan rates ranging from 5 to 100 mV s^{-1}.

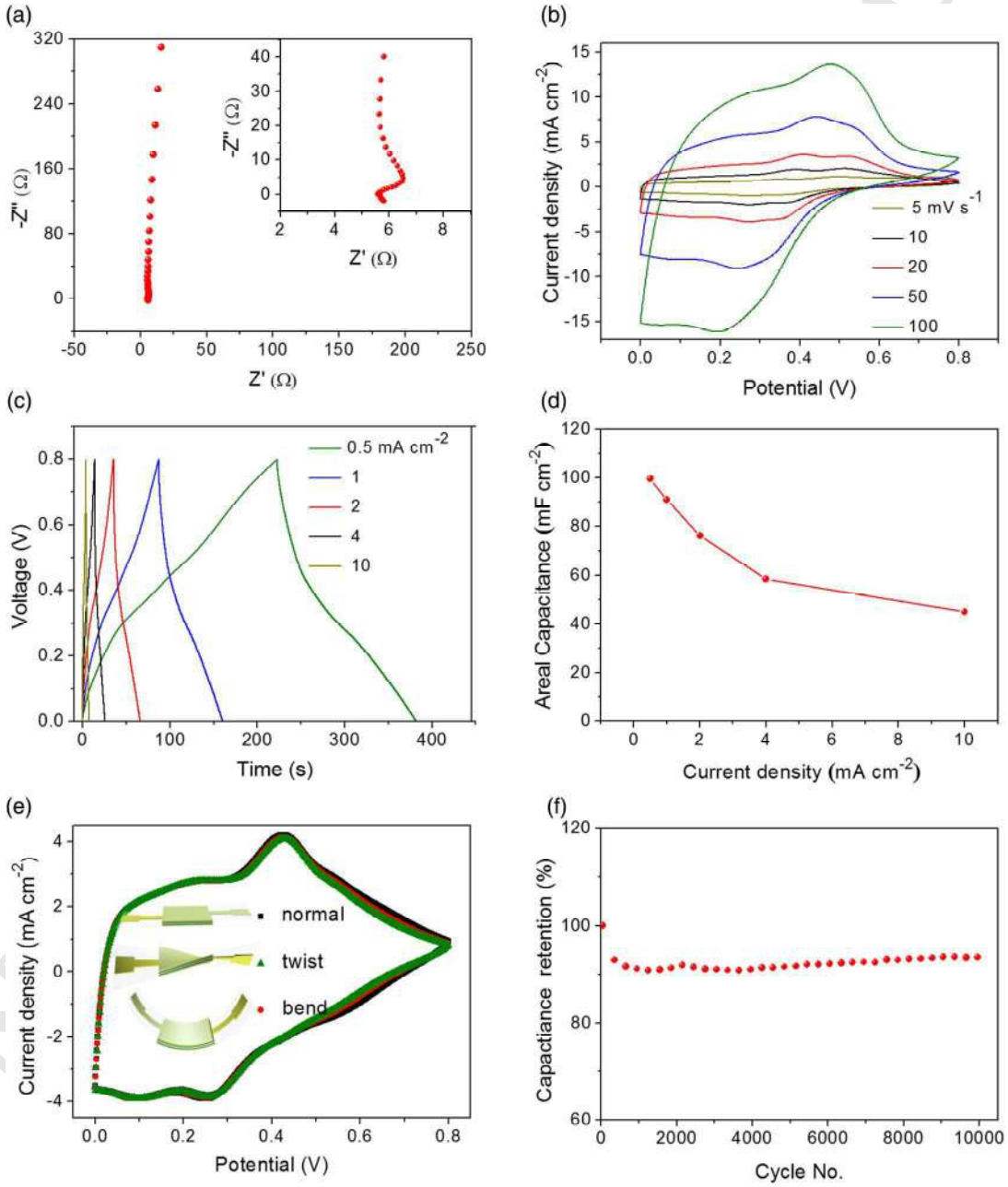

Figure 4. a) Impedance plot in the frequency range of 10 mHz to 100 kHz. b) CV curves of the SC at different scan rates. c) GCD curves collected at different current densities for SC. d) The areal capacitances of flexible solid-state supercapacitors depending on different current densities. e) CV curves for the SC under three different states (flatting, bending, and twisting). f) Cycling performance of the SC at a current density of 5 mA cm^{-2}.

As expected, the shapes are not ideal rectangles but present some characteristic redox peaks of PANI, originating from the transformation among the leucoemeraldine base, the emeraldine salt, and the pernigraniline base.[16a] However, the shape of the CV curves apparently becomes deformed with an increase in scan rates, demonstrating the decline of the capacitive performance. As the scanning rate increases, the velocity of ions migrating from the PVA/H_2SO_4 gel electrolyte to the electrode–electrolyte interface accelerates, whereas the diffusion rate of the electrolyte from the solid–liquid interface to the electrode material is not enough to meet the electrochemical reaction of the electrode material, thus leading to the accumulation of a large number of ions near the electrode–electrolyte interface.[23] Moreover, it can be clearly observed from the CV curves that the current density of the device increases with the increase in the scan rate, indicating a promising rate capability. This can be ascribed to the interconnected porous framework of CPHs and a good conductivity. To further confirm the capacitive behavior of the pp-CPHs, the GCD test within a potential window of 0–0.8 V is carried out as shown in Figure 4c. Consistently, the linear profile of GCD curves and their shape like a triangle demonstrate a relatively good charge–discharge performance based on pp-CPHs. According to Equation (1), the corresponding areal capacitances are calculated to be 99.5, 91, 76.25, 58.5, and 45 mF cm^{-2}, respectively (Figure 4d). To verify the practicability of the device based on pp-CPHs, we compare the CV curves of our device under its flat, bent, and twisted states measured at 2 mV s^{-1} (Figure 4e). The electrochemical performance of such SCs almost remains nearly constant under these three conditions.

Figure 4f shows the cycling performance of the SCs. The device maintains 93.5% of its initial capacitance performance after 10 000 charge–discharge cycles at 5 mA cm^{-2}, indicating that the SCs have an excellent cycling stability and a high reversibility during repeated charge–discharge cycles. Such an outstanding capacitive performance can be attributed to the exceptional electrical robustness of the hierarchically nanostructured 3D network, which is conducive to the insertion and transmission of ions.[24] In addition, we use gold as the collector, which also improves the circulating stability of the equipment to some extent. To investigate the scope of the pp-CPH-based device, we varied the pp-CPHs loading on electrodes from 0.20 to 1.02 mg (**Figure 5**a) and examined the obtained pp-CPH electrodes using the GCD method with the current densities of 1 A g^{-1} and 1 mA cm^{-2} (Figure 5c,d). Remarkably, when the pp-CPH loading increases, the specific capacitance of the pp-CPH electrode remains basically the same, while the areal capacitance gradually increases (Figure 5b). The pp-CPH loading on electrodes is nearly directly proportional to the areal capacitance, and the loading roughly changed linearly with the areal capacitance. The highest areal capacitance is measured with 1.02 mg pp-CPH loading, reaching 135 mF cm^{-2} based on the mass of pp-CPHs. Therefore, the requirements of a high specific capacitance and

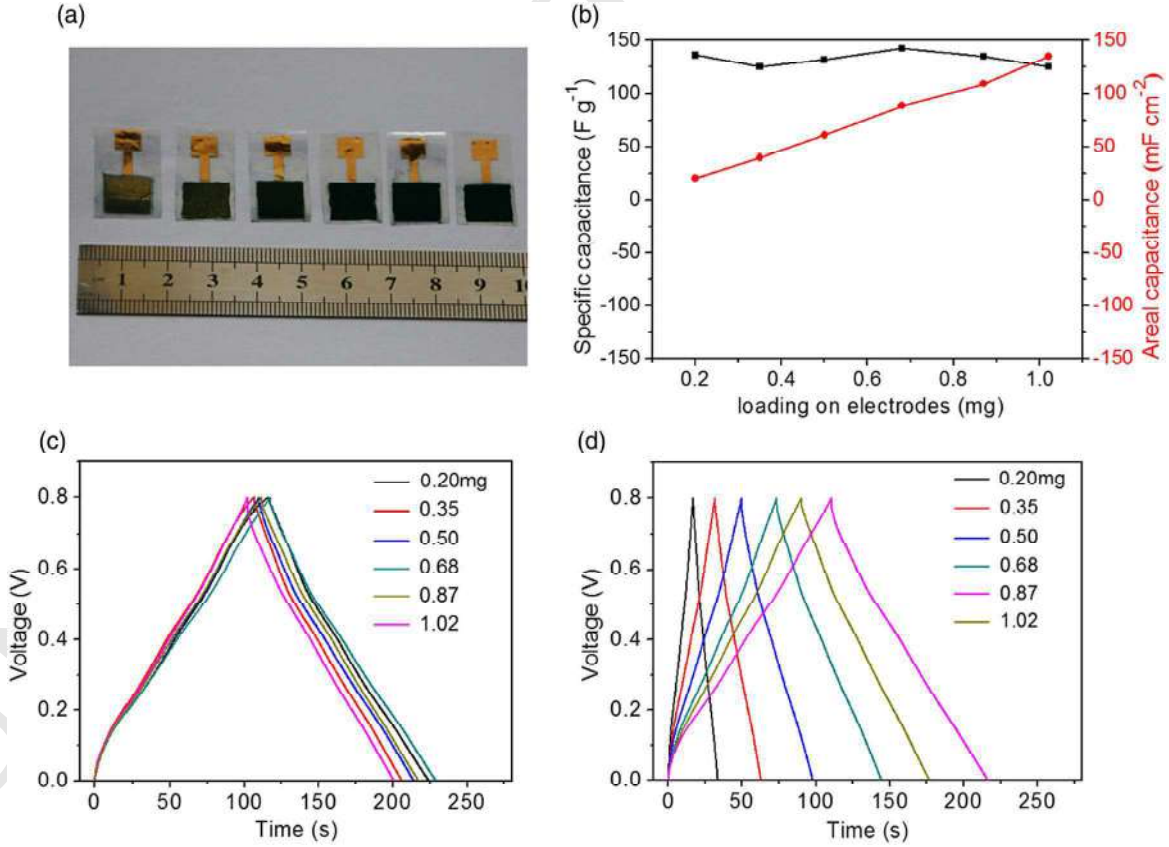

Figure 5. a) Digital image of different pp-CPHs loading on electrodes. b) Specific capacitance and areal capacitance of pp-CPHs electrodes with different loadings. GCD curves obtained for different pp-CPH loadings from 0.20 to 1.02 mg at the current densities of c) 1 mA cm^{-2} and d) 1 A g^{-1}, respectively.

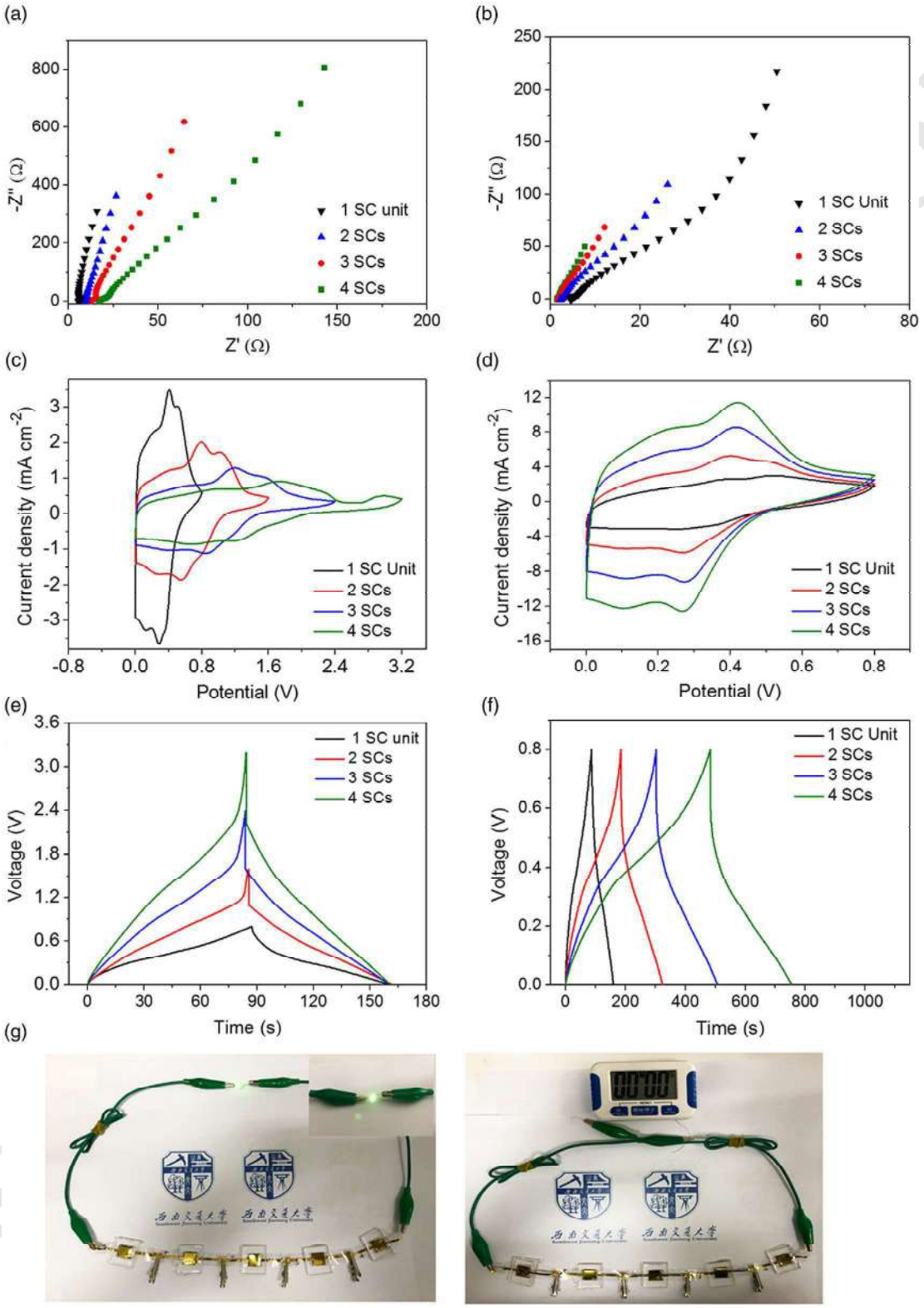

Figure 6. Nyquist plots of the increasing number of SCs connected a) in series and b) in parallel, obtained at a frequency loop from 10 mHz to 10 kHz. c) CV and e) GCD of SCs (1, 2, 3, 4 serially connected SCs), measured at 20 mV s^{-1} and 1 mA cm^{-2}, respectively. d) CV and f) GCD of SCs (1, 2, 3, 4 parallelly connected SCs). g) Photos of a green LED powered by the five SCs in series.

high areal capacitance are balanced when the pp-CPH loading is about 1.02 mg.

To demonstrate the practical applications of the pp-CPH-based supercapacitor, the parallel and series connecting circuit of as-prepared devices are systematically studied. The internal resistance (≈5.06 Ω) is superimposed after SC units were connected in the series (≈17.12 Ω), as shown in **Figure 6**a. The inner resistance of the four parallelly connected SCs (≈1.33 Ω) is probably a quarter of a single SC unit (≈5.06 Ω) obtained by Nyquist plots, as shown in Figure 6b. These characteristics mentioned earlier indicate that our devices have excellent uniformity. From the CV curves in Figure 6c, an enhanced potential range by SC units connected in a series can be observed. Moreover, the charging–discharging time of the series device is basically the same as that of the single device at the same current density (Figure 6e). As shown in Figure 6d,f, the output current of the four parallelly connected SC units increases by a factor of four compared with a single SC unit. Meanwhile, the potential window of the parallel device increases as the number of parallel connections increases. To meet the demand for power and energy, the current and its potential window can be extended by connecting SC units in parallel or in series. Finally, we used a series device to light up a green light-emitting diode (LED, 3.2 V) and timer (3 V) (Figure 6g), demonstrating its practical potential as a flexible energy storage device.

4. Conclusion

In summary, the hierarchically nanostructured pp-CPH-based flexible all-solid-state supercapacitors were prepared via a simple massively all-sprayable spraying approach. Due to uniquely structured design of pp-CPHs, such supercapacitors with a sandwich structure and PVA/H_2SO_4 gel electrolytes achieve a high areal capacitance (91 mF cm^{-2} at 1 mA cm^{-2}) and an excellent cycling stability (93.5% capacitance retention over 10 000 charge–discharge cycles). In addition, those as-prepared supercapacitors showed an outstanding flexible performance (in the bent and twisted states), attributing to sensationally compression stability of the 3D porous pp-CPHs. Furthermore, the excellent series or parallel connection performances remarkably show the practical integration of this device. All the results suggest that such pp-CPH-based flexible all-solid-state supercapacitors have a good potential application as wearable supercapacitors. Due to the open channels of 3D layered nanostructures, our pp-CPH materials exhibit a better cyclic stability than PANI hydrogels reported previously, which has a certain reference value for the design of new 3D network hydrogels.

Acknowledgements

X.C. and Y.H. contributed equally to this work. The authors are thankful to Analytical and Testing Center of Southwest Jiaotong University for supporting the SEM measurements. This work is supported by the National Natural Science Foundation of China (No. 51602265), the Scientific and Technological Projects for International Cooperation of Sichuan Province (No. 2017HH0069), the Special Fund of China Postdoctoral Science Foundation (No. 2018T110992), the Fundamental Research Funds for the Central Universities of China (No. 2682016CX074), and the Independent Research Project of State Key Laboratory of Traction Power (No. 2017TPL_Z04).

Conflict of Interest

The authors declare no conflict of interest.

Keywords

conductive polymer hydrogels, flexible, phytic acid, polyaniline, spraying, supercapacitors

Received: December 3, 2018
Revised: March 2, 2019
Published online:

[1] a) X. Lu, M. Yu, G. Wang, Y. Tong, Y. Li, *Energy Environ. Sci.* **2014**, *7*, 2160; b) T. S. Kim, J. E. Lim, M. S. Oh, J. K. Kim, *J. Power Sources* **2017**, *361*, 15; c) C. Yan, W. Deng, L. Jin, T. Yang, Z. Wang, X. Chu, H. Su, J. Chen, W. Yang, *ACS Appl. Mater. Interfaces* **2018**, *10*, 41070; d) S. Dai, J. Liu, C. Wang, X. Wang, Y. Xi, D. Wei, *Energy Technol.* **2016**, *4*, 1450.
[2] a) F. Liu, B. Zhang, H. Su, H. Zhang, L. Zhang, W. Yang, *Nanotechnology* **2016**, *27*, 355603; b) H. Huang, H. Su, H. Zhang, L. Xu, X. Chu, C. Hu, H. Liu, N. Chen, F. Liu, W. Deng, B. Gu, H. Zhang, W. Yang, *Adv. Electron. Mater.* **2018**, *4*, 1800179.
[3] a) J. Han, K. Wang, W. Liu, C. Li, X. Sun, X. Zhang, Y. An, S. Yi, Y. Ma, *Nanoscale* **2018**, *10*, 13083; b) H. Zhang, H. Su, L. Zhang, B. Zhang, F. Chun, X. Chu, W. He, W. Yang, *J. Power Sources* **2016**, *331*, 332. c) L. Tian, M. Liu, D. Zhu, L. Gan, C. Tao, *Adv. Mater.* **2018**, *30*, 1705489.
[4] a) Z. Tai, X. Yan, Q. Xue, *J. Electrochem. Soc.* **2012**, *159*, A1702; b) K. Wang, W. Zou, B. Quan, A. Yu, H. Wu, P. Jiang, Z. Wei, *Adv. Energy Mater.* **2011**, *1*, 1068.
[5] Y. Zhao, B. Liu, L. Pan, G. Yu, *Energy Environ. Sci.* **2013**, *6*, 2856.
[6] a) Z. Xu, X. Zhuang, C. Yang, J. Cao, Z. Yao, Y. Tang, J. Jiang, D. Wu, X. Feng, *Adv. Mater.* **2016**, *28*, 1981; b) S.-X. Wang, S. Chen, Q. Wei, X. Zhang, S. Y. Wong, S. Sun, X. Li, *Chem. Mater.* **2014**, *27*, 336; c) Y.-Y. Peng, B. Akuzum, N. Kurra, M.-Q. Zhao, M. Alhabeb, B. Anasori, E. C. Kumbur, H. N. Alshareef, M.-D. Ger, Y. Gogotsi, *Energy Environ. Sci.* **2016**, *9*, 2847; d) Y. Xie, D. Wang, J. Ji, *Energy Technol.* **2016**, *4*, 714; e) X. Wu, M. Lian, *J. Power Sources* **2017**, *362*, 184.
[7] W. Li, F. Gao, X. Wang, N. Zhang, M. Ma, *Angew. Chem., Int. Ed. Engl.* **2016**, *55*, 9196.
[8] X. Jiang, Y. Cao, P. Li, J. Wei, K. Wang, D. Wu, H. Zhu, *Mater. Lett.* **2015**, *140*, 43.
[9] Y. Xie, C. Xia, H. Du, W. Wang, *J. Power Sources* **2015**, *286*, 561.
[10] L. Du, P. Yang, X. Yu, P. Liu, J. Song, W. Mai, *J. Mater. Chem. A* **2014**, *2*, 17561.
[11] A. M. Wan, S. Inal, T. Williams, K. Wang, P. Leleux, L. Estevez, E. P. Giannelis, C. Fischbach, G. G. Malliaras, D. Gourdon, *J. Mater. Chem. B* **2015**, *3*, 5040.
[12] a) E. Armelin, M. M. Pérez-Madrigal, C. Alemán, D. D. Díaz, *J. Mater. Chem. A* **2016**, *4*, 8952; b) X. Dai, Y. Zhang, L. Gao, T. Bai, W. Wang, Y. Cui, W. Liu, *Adv. Mater.* **2015**, *27*, 3566.
[13] a) T. Aida, E W. Meijer, S I. Stupp, *Science* **2012**, *335*, 813; b) B. Bao, J. Hao, X. Bian, X. Zhu, K. Xiao, J. Liao, J. Zhou, Y. Zhou, L. Jiang, *Adv. Mater.* **2017**, *29*, 1702926.

[14] a) Y. Shi, L. Pan, B. Liu, Y. Wang, Y. Cui, Z. Bao, G. Yu, *J. Mater. Chem. A* **2014**, *2*, 6086; b) M. M. Pérez-Madrigal, F. Estrany, E. Armelin, D. D. Díaz, C. Alemán, *J. Mater. Chem. A* **2016**, *4*, 1792.
[15] G P. Hao, F. Hippauf, M. Oschatz, F M. Wisser, A. Leifert, W. Nickel, N. Mohamed-Noriega, Z. Zheng, S. Kaskel, *ACS Nano* **2014**, *8*, 7138.
[16] a) X. Chu, H. Zhang, H. Su, F. Liu, B. Gu, H. Huang, H. Zhang, W. Deng, X. Zheng, W. Yang, *Chem. Eng. J.* **2018**, *349*, 168; b) S. R. Kwon, J.-W. Jeon, J. L. Lutkenhaus, *RSC Adv.* **2015**, *5*, 14994; c) F. Guo, Q. Liu, H. Mi, *Mater. Lett.* **2016**, *163*, 115; d) H. Heydari, M. B. Gholivand, *New J. Chem.* **2017**, *41*, 237.
[17] a) L. Pan, G. Yu, D. Zhai, H. R. Lee, W. Zhao, N. Liu, H. Wang, B. C. Tee, Y. Shi, Y. Cui, Z. Bao, *Proc. Natl. Acad. Sci. U. S. A.* **2012**, *109*, 9287. b) J. G. Wang, H. Liu, H. Liu, W. Hua, M. Shao, *ACS Appl. Mater. Interfaces* **2018**, *10*, 11888.
[18] a) H. Guo, W. He, Y. Lu, X. Zhang, *Carbon* **2015**, *92*, 133; b) Y. Xu, Z. Lin, X. Huang, Y. Liu, Y. Huang, X. Duan, *ACS Nano* **2013**, *7*, 4042.
[19] H. Kuang, Q. Cao, X. Wang, B. Jing, Q. Wang, L. Zhou, *J. Appl. Polym. Sci.* **2013**, *130*, 3753.
[20] W. Yang, Z. Gao, N. Song, Y. Zhang, Y. Yang, J. Wang, *J. Power Sources* **2014**, *272*, 915.
[21] A. Olad, H. Gharekhani, *Prog. Org. Coat.* **2015**, *81*, 19.
[22] B.-S. Yin, S.-W. Zhang, Q.-Q. Ren, C. Liu, K. Ke, Z.-B. Wang, *J. Mater. Chem. A* **2017**, *5*, 24942.
[23] a) X. Shi, Z. S. Wu, J. Qin, S. Zheng, S. Wang, F. Zhou, C. Sun, X. Bao, *Adv. Mater.* **2017**, *29*, 1703034; b) Y. Yin, C. Liu, S. Fan, *J. Phys. Chem. C* **2012**, *116*, 26185.
[24] a) M. Li, Z. Tang, M. Leng, J. Xue, *Adv. Funct. Mater.* **2014**, *24*, 7495; b) L.-X. Yuan, Z.-H. Wang, W.-X. Zhang, X.-L. Hu, J.-T. Chen, Y.-H. Huang, J. B. Goodenough, *Energy Environ. Sci.* **2011**, *4*, 269.